Analog Integrated Circuits and Signal Processing, 18, 243–254 (1999)

Silicon Retina with Adaptive Filtering Properties

SHIH-CHII LIU

Institute for Neuroinformatics, Eth/Uniz, Winterthurerstr 190, CH-8051 Zurich, Switzerland
shih@ini.phys.ethz.ch

Received April 3, 1997; Revised September 25, 1997

Abstract. This paper describes a small, compact circuit, the retino-laminar (RL) circuit, that captures the temporal and adaptation properties both of the photoreceptor and of the laminar layers of the fly. The RL circuit uses only six transistors and two capacitors. The circuit is operated in the subthreshold domain; it has a low DC gain and a high transient gain. The adaptation time constant of the RL circuit can be controlled via an external bias. Its temporal filtering properties change with the background intensity and with the signal-to-noise ratio. The frequency response of the circuit shows that, in the frequency range of 1 to 100 Hz, the circuit response goes from highpass filtering under high light levels to lowpass filtering under low light levels (i.e., when the signal-to-noise ratio is low).

Key Words: silicon retina, photoreceptor, adaptive filtering, adaptation

1. Background

The first two layers in the fly visual system are the retina layer and the laminar layer. The photoreceptors in the retina synapse onto the monopolar cells in the laminar layer. The photoreceptors adapt to the background intensity, and use this adaptation as a form of gain control in maintaining a high response to transient signals. The laminar layer performs band-pass filtering under high background intensities, and reverts to lowpass filtering in the case of low background intensities where the signal-to-noise (S/N) ratio is low.

The Delbrück silicon receptor circuit [1] modeled closely the step responses and the adaptation responses of the biological receptors. With two additional transistors, the **retino-laminar (RL)** circuit described here captures the properties of both the photoreceptor layer (i.e., the adaptation properties and phototransduction) and the cells in the laminar layer (i.e., the adaptive filtering). The time constant of the circuit is controllable via an external bias, and the adaptation behavior of the circuit over different background intensities is more symmetrical than that of Delbrück's photoreceptor circuit [1].

2. Circuit Description

The RL circuit is shown in Fig. 1. I have replaced the adaptive element in Delbrück's photoreceptor circuit [1] by a nonlinear resistor consisting of a pFET transistor, Q_1. The implementation of a floating, voltage-controlled resistor has been described earlier by Banu and Tsividis [3]. The bias for the pFET, V_b, is generated by Q_3 and Q_4. An external bias voltage, V_m controls Q_3. Hence, we can control the conductance of Q_1 via V_m. I give a brief description of the circuit operation here; details are presented in [1]. The receptor voltage, V_r, is clamped to the voltage needed to sink the current sourced by Q_6, which is biased by an external bias, V_u. Transistors Q_2 and Q_6 form a high-gain, inverting amplifier. The value of V_{pl} sits at the voltage required for Q_5 to supply the photocurrent. The feedback transistor, Q_5, is operated in subthreshold so that V_r is logarithmic in the photocurrent. When the photocurrent increases, the change in V_r leads to a large change at the output, V_1. This change in V_1 is capacitively coupled through the capacitive divider, consisting of C_1 and C_d, into V_{pl}, so that Q_5 supplies the extra increase in photocurrent.

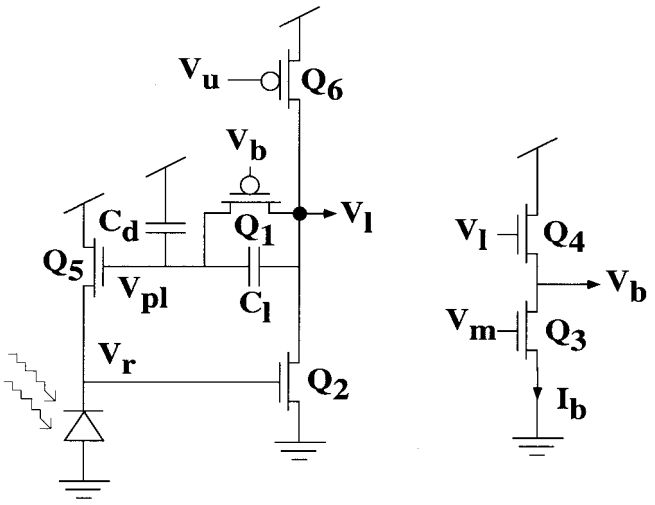

Fig. 1. Circuit diagram of retino-laminar circuit. The feedback consists of a resistor implemented by a pFET transistor, Q_1. The conductance of the resistor is controlled by the external bias, V_m.

3. Variants of the Retino-laminar Circuit

In this paper, I describe two variants of this circuit: RL_1 and RL_2. The first variant, RL_1, is similar to the circuit in Fig. 1, except that a cascode transistor has been added to the circuit as shown in Fig. 2. The second variant, RL_2 (shown in Fig. 9), has the same basic form as RL_1, except that the biasing circuit is different. Both circuits use only six transistors plus two capacitors, C_1 and C_d. The size of the layout of each of the variants is approximately 95 μm $\times$ 100 μm.

3.1. RL_1

The variant RL_1 is shown in Fig. 2. The extra cascode transistor increases the bandwidth of the circuit. The dependence of the temporal responses and adaptation

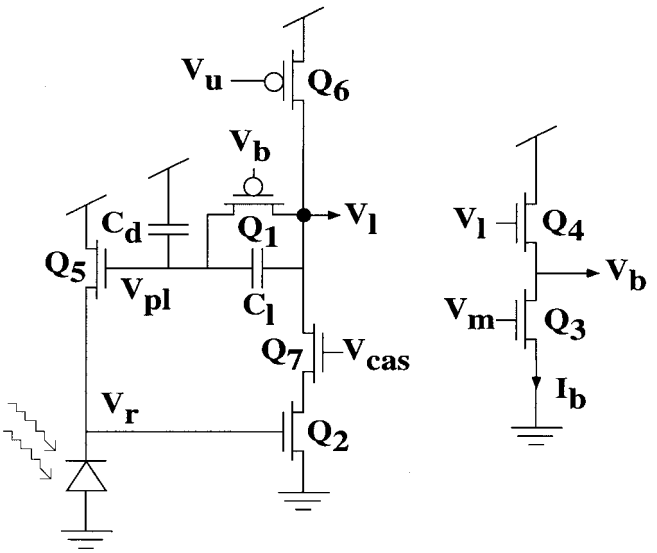

Fig. 2. Circuit diagram of the variant, RL_1. The circuit is the same as that in Fig. 1, except that we added a cascode transistor, Q_7, to decrease the Miller capacitance at the node, V_r.

properties of this circuit on the background intensity (or signal-to-noise ratio) are expounded in Sections 3.1.1 through 3.1.4.

3.1.1. Transfer Function. We first solve for the transfer function of the circuit by writing the KCL equations at the nodes, v_r, v_{pl}, and v_l, in the small-signal model shown in Fig. 3:

$$\dot{v_{pl}}C_{\mathrm{d}} + C_1(\dot{v_{pl}} - \dot{v_l}) + g_a(v_{pl} - v_l) = 0 \quad (1)$$

$$g_{m2}v_r + v_l g_d + C_1(\dot{v_l} - \dot{v_{pl}}) + g_a(v_l - v_{pl}) = 0 \quad (2)$$

$$i_{in} + C_r\dot{v_r} = g_{m5}(v_{pl} - v_r/\kappa) \quad (3)$$

where C_r is the parasitic capacitance at the node V_r, g_a is the output conductance of Q_1, and g_s is the source conductance of Q_5. Taking the Laplace transform of equations (1) through (3), we get

$$sv_{pl}C_{\mathrm{d}} + sC_1(v_{pl} - v_l) + g_a(v_{pl} - v_l) = 0 \quad (4)$$

$$g_{m2}v_r + v_l g_d + sC_1(v_l - v_{pl}) + g_a(v_l - v_{pl}) = 0 \quad (5)$$

$$i_{in} + sC_r v_r = g_{m5}(v_{pl} - v_r/\kappa) \quad (6)$$

From equations (4) through (6), we derive the transfer function–(v_l/i_{in}):

$$\frac{v_l}{i_{in}} = \frac{1}{g_{m5}}\left[\frac{\frac{s(\tau_{ld}+\tau_l)+g_a/g_{m2}}{s\tau_l+g_a/g_{m2}}}{(s\tau_r + 1/\kappa)\left(\frac{1}{A_{\mathrm{amp}}} + s\tau_{ld} + \frac{s\tau_{ld}}{A_{\mathrm{amp}}(s\tau_l+g_a/g_{m2})}\right) + 1}\right] \quad (7)$$

where the time constants, τ_l, τ_r, τ_{ld}, and the amplifier gain, A_{amp}, are defined as follows:

$$\tau_l = \frac{C_1}{g_{m2}};\ \tau_r = \frac{C_r}{g_{m5}};\ \tau_{ld} = \frac{C_{\mathrm{d}}}{g_{m2}};\ A_{\mathrm{amp}} = \frac{g_{m2}}{g_d}$$

The low-frequency gain of the circuit is then

$$\frac{v_l/U_T}{i_{in}/I_{ph}} = \frac{1}{\kappa}\frac{A_{\mathrm{amp}}}{1 + \kappa A_{\mathrm{amp}}}$$

and the circuit has a zero at

$$z_0 = -\frac{g_a}{C_{\mathrm{d}} + C_1}$$

The frequency-response curves in Fig. 4 were measured from the fabricated circuit over five decades of background intensity. The input to the circuit was from a sine-wave-modulated red LED source. The number next to each curve is the log intensity of the mean value; 0 log is the intensity of a red LED. I obtained the remaining curves by interposing neutral density filters between the LED source and the chip. Fig. 4 shows that, in the range of 1 to 100 Hz, the circuit is a bandpass filter at high light levels, and reduces to a lowpass filter at low light levels. For each frequency curve, the gain is flat in the middle, and is given by $A_{\mathrm{cl}} = (C_1 + C_{\mathrm{d}})/C_1$. The change in the cutoff frequencies with the background intensity is analyzed in Section 3.1.2.

3.1.2. I–V Relationship. Here, we analyze the dependence of the cutoff frequencies of the circuit on the background intensity. The equation for the current through Q_1 can be written as

$$\begin{aligned} I &= I_{op}e^{-\kappa_p V_{\mathrm{b}}}(e^{(\overline{V}+\Delta V/2)} - e^{(\overline{V}-\Delta V/2)}) \\ &= I_{op}e^{-\kappa_p V_{\mathrm{b}}}e^{\overline{V}}(e^{\Delta V/2} - e^{-\Delta V/2}) \\ &= 2I_{op}e^{-\kappa_p V_{\mathrm{b}}}e^{\overline{V}}\sinh(\Delta V/2)) \end{aligned} \quad (8)$$

where $\overline{V} = (V_1 + V_{\mathrm{pl}})/2$ and $\Delta V = V_1 - V_{\mathrm{pl}}$. The term $\overline{V}$ corresponds to the common-mode voltage, and ΔV corresponds to the differential-mode voltage across Q_1. The exponential relationship for equation (8) is for a transistor operating in subthreshold, where I_{op} is the quiescent leakage current of the pFET transistor, and κ_p is the effectiveness of the gate in controlling the surface potential of the channel of the pFET.

The KCL equation for the bias circuit consisting of Q_3 and Q_4 is given by

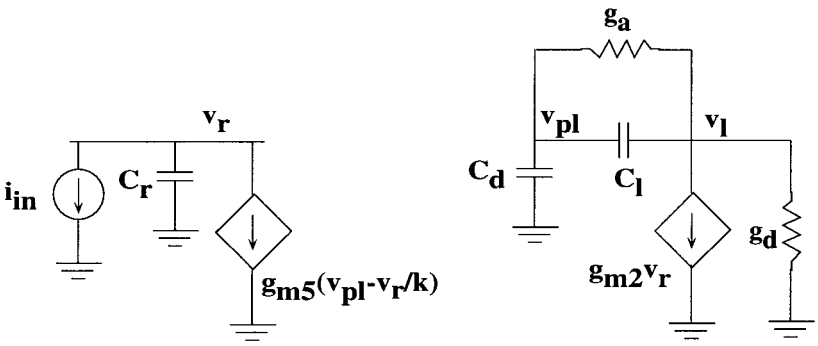

Fig. 3. Small-signal model of the circuit shown in Fig. 2. Here, C_{r} is the parasitic capacitance at the node, V_{r}.

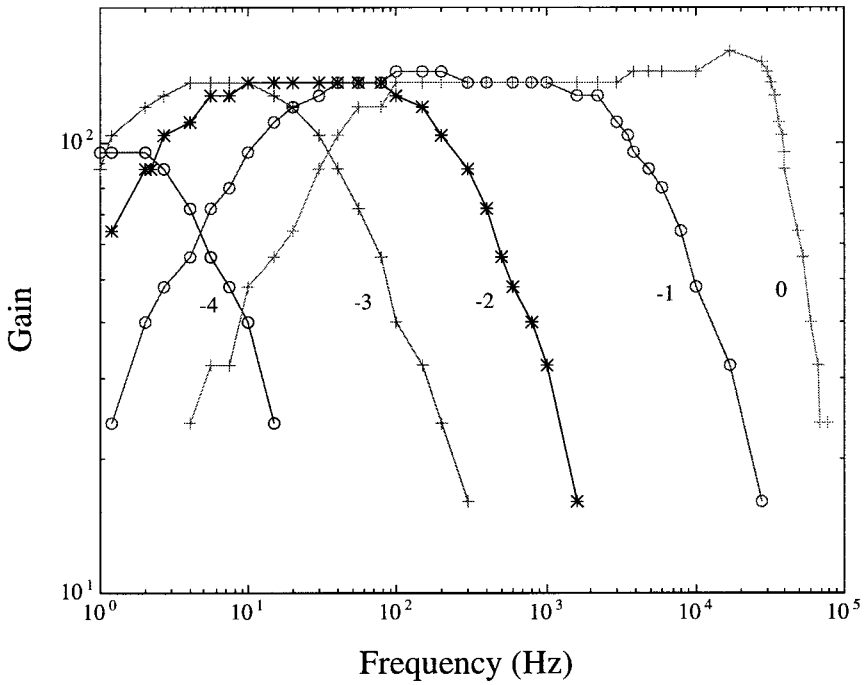

Fig. 4. Frequency plot of the RL_1 circuit over five decades of background intensity. The number next to each curve corresponds to the log intensity of the mean value; 0 log corresponds to the intensity of a red LED. The plot shows that, in the range of 1 to 100 Hz, the circuit is a bandpass filter at high light levels, and reduces to a lowpass filter at low light levels.

$$I_b = I_{on} e^{\kappa_n(\overline{V}+\Delta V/2)} e^{-V_b} \tag{9}$$

where $V_1 = \overline{V} + \Delta V/2$, I_{on} is the quiescent leakage current of the nFET transistor, and κ_n is the effectiveness of the gate in controlling the surface potential of the channel of the nFET. We rearrange the terms in equation (9) to solve for $e^{-\kappa_p V_b}$:

$$e^{-\kappa_p V_b} = \left(\frac{I_b}{I_{on}}\right)^{\kappa_p} e^{-\kappa_n\kappa_p(\overline{V}+\Delta V/2)} \tag{10}$$

Substituting equation (10) into equation (8), we get the I–V relationship for Q_1:

$$I = 2I_{op}\left(\frac{I_b}{I_{on}}\right)^{\kappa_p} e^{(1-\kappa_n\kappa_p)\overline{V}} e^{-\kappa_n\kappa_p\Delta V/2} \sinh(\Delta V/2) \tag{11}$$

The I–V curves as measured for several common-mode voltages are shown in Fig. 5. The curves are asymmetrical because Q_1 acts like a resistor when V_1 is higher than V_{pl}, and acts like a diode when V_1 is less than V_{pl}. Interestingly, an increase in the voltage, V_1, leads to a decrease in κ_p of Q_1 and to an increase in κ_n of Q_4. Hence, the change in the κ effects tend to cancel out each other.

We can compute the dependence of the I–V relationship for Q_1 on I_{ph} by substituting for $\overline{V} = (V_1 + V_{pl})/2 = V_{pl} + \Delta V/2$ in equation (11). We also know that V_{pl} biases Q_5, which supplies the photocurrent, I_{ph}. Since $I_{ph} = I_{on} e^{\kappa_n V_{pl} - V_r}$,

$$\left(\frac{I_{ph} e^{V_r}}{I_{on}}\right)^{1/\kappa_n} = e^{V_{pl}} \tag{12}$$

Substituting equation (12) into equation (11), we get

$$I = I_\alpha I_{ph}^{(1-\kappa_n\kappa_p)/\kappa_n} e^{(1-2\kappa_n\kappa_p)\Delta V/2} \sinh(\Delta V/2) \tag{13}$$

where

$$I_\alpha = 2I_{op}\left(\frac{I_b}{I_{on}}\right)^{\kappa_p}\left(\frac{e^{V_r}}{I_{on}}\right)^{(1-\kappa_n\kappa_p)/\kappa_n}$$

Equation (13) shows that the conductance, g_a, of Q_1, in Fig. 3, is proportional to the background intensity, I_{ph}. As I_{ph} increases, g_a increases, so the cutoff frequencies shift to the right, as seen in Fig. 4. If we compare both the ''0'' curve and the '' -1'' curve, we can see that the cutoff frequencies are approximately different by a factor of 10. The exponent of I_{ph}, $(1 - \kappa_n\kappa_p)/\kappa_n$, in equation (13) is then approximately equal to 1. Since the κ values change with the current through the transistor, the exponent also changes. The different values of the exponent with I_{ph} can be seen

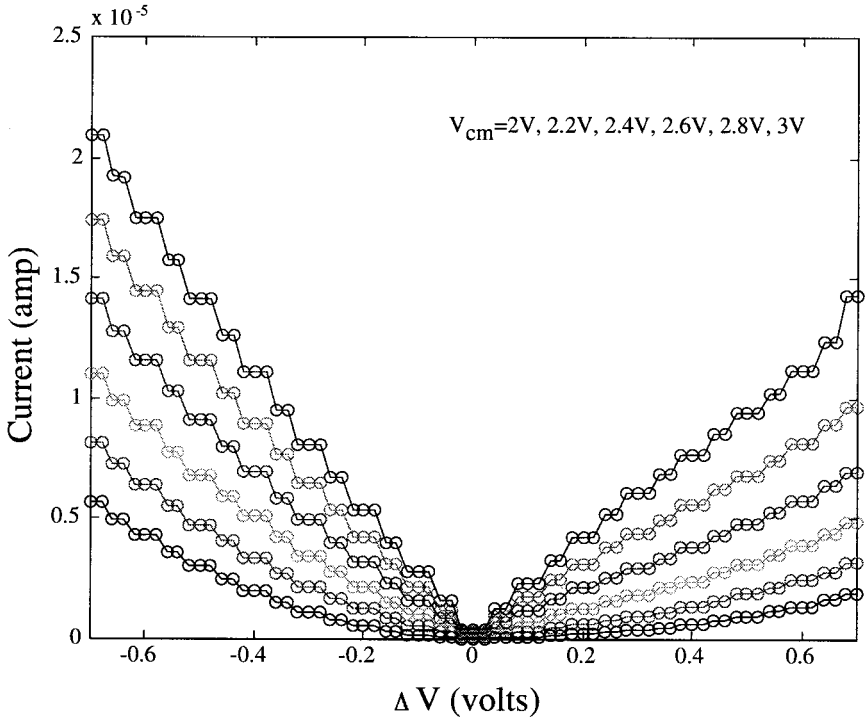

Fig. 5. Measured I–V curves of Q1 for six different common-mode voltages.

from the different amounts of shifts in the cutoff frequencies of the curves.

3.1.3. Temporal Responses. The dependence of the temporal filtering of the circuit on the background intensity, for a fixed value of V_m, is shown in Fig. 6. The input stimulus to the circuit is a square-wave-modulated LED with a contrast of 0.15, where the contrast is defined as $(I_{max} - I_{min})/(I_{max} + I_{min})$. The data in Fig. 6 show the adaptive filtering of the circuit over five decades of background intensity. The temporal responses observed in these circuits are comparable to the contrast responses recorded from the LMCs by Juusola and colleagues [2]. The time constant of the circuit increases as the background intensity decreases. This dependence of the temporal filtering on the background intensity is analogous to the dependence of the spatial filtering on the background intensity in both the vertebrate retina and the invertebrate retina. The change in the time constant of the circuit is due to the change in the conductance, g_a, as the background intensity changes. The conductance, g_a, is greater at high background intensities because of the increased body effect at Q_4 due to a higher source voltage.

3.1.4. Adaptation Properties. We can view the retino-laminar circuit as a version of the Delbrück circuit with an adaptation time constant that is set by an external bias. In the Delbrück circuit, the adaptation time constant is predetermined at the design phase and by process parameters. In Fig. 7, we compare the adaptation properties of RL_1 with those of Delbrück's circuit. The input stimulus consists of a square-wave modulated LED source of contrast 0.18. We take the circuit from dark to light conditions, and back, by using neutral density filters. The top curve corresponds to the response from the RL_1 circuit, and the bottom curve corresponds to the response from the Delbrück circuit. The RL_1 circuit adapts symmetrically, when it goes from light to dark conditions and back. In contrast, Delbrück's circuit shows an asymmetrical adaptative behavior; it adapts more slowly when it goes from dark to light conditions. The curve also shows that the adaptation time constant of the Delbrück circuit, unexpectedly, depends on the background intensity. The time constant of the adaptive element probably changes because the minority carriers that generated in the photodiode area migrate to the well in which the adaptive element sits, and alter the conductance of this element.

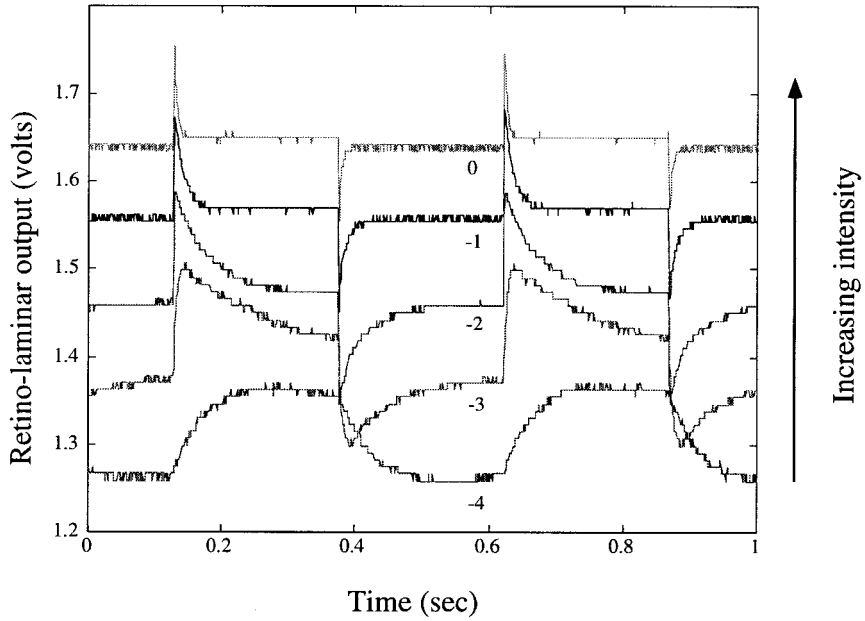

Fig. 6. Temporal responses of RL_1 over five decades of background intensity. The input stimulus is a red blinking LED of contrast 0.15. The circuit acts as a highpass filter (that is, a differentiator) at high intensities, and as a lowpass filter as the intensity drops.

As described earlier, the adaptation time constant of the RL_1 circuit can be controlled via the bias voltage, V_m. Fig. 8 shows the adaptation properties of the circuit for two different values of V_m. The top curve in the figure corresponds to a larger value of V_m, and hence to an increased conductance, g_a, or to a decreased time constant. We can see that the adaptation time constant is smaller for the top curve

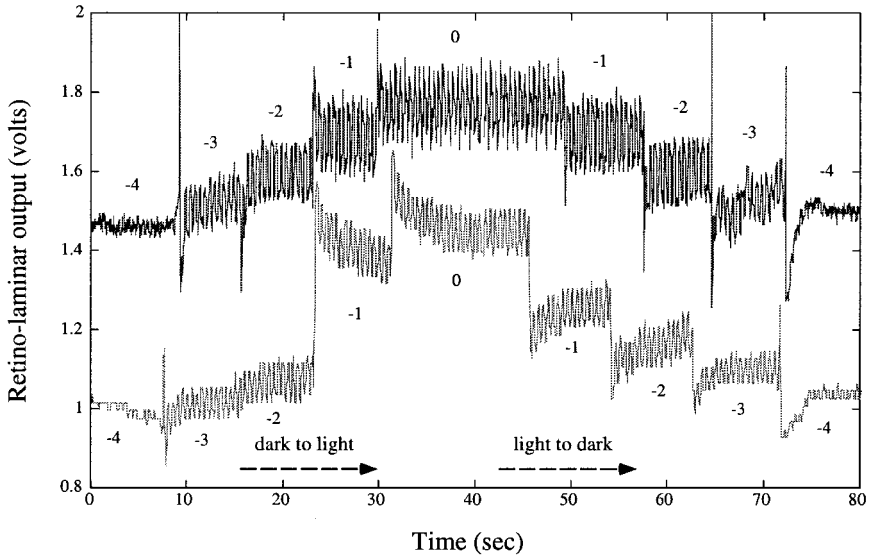

Fig. 7. Plots of adaptation responses of RL_1 and of Delbrück's circuit. The input stimulus is a square-wave modulated LED of contrast 0.18. The bottom curve corresponding to Delbrück's receptor has been shifted down so that we can compare the two curves. The adaptation response of the RL_1 circuit is more symmetrical than that of Delbrück's circuit when the circuit goes from dark to light conditions and back.

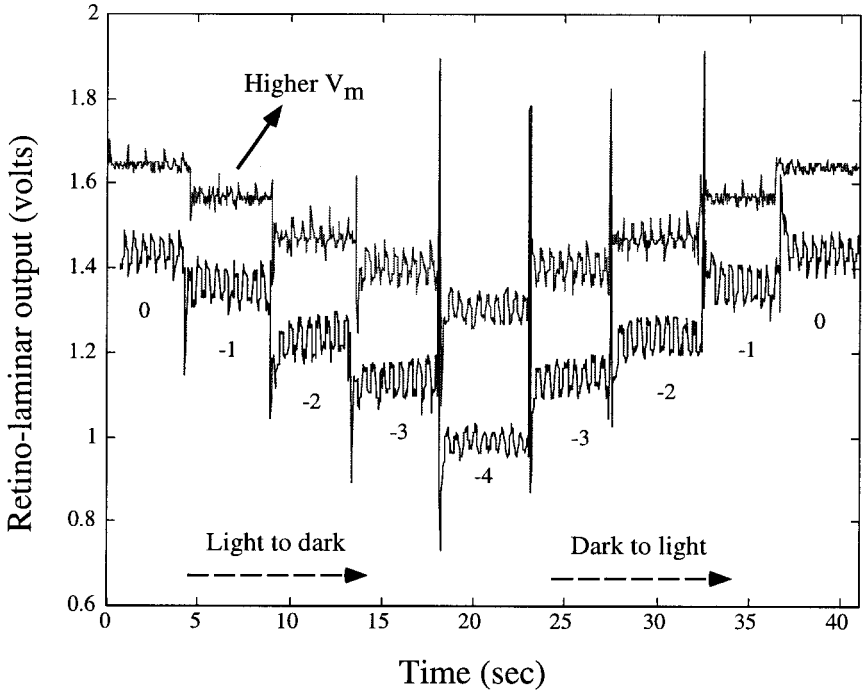

Fig. 8. Adaptation responses of the RL_1 circuit for two values of V_m. The curves show how the adaptation time constant of the circuit changes with V_m (or I_b), when the circuit goes from dark to light conditions and back. The bottom curve corresponds to a smaller value of V_m, and the curve has been shifted down by 0.2 V for ease of comparison.

than for the bottom curve. Fig. 8 also shows that the adaptation time constant is less affected by changes in V_m when the circuit goes from light to dark than when it goes from dark to light conditions. This asymmetry comes about because Q_4 acts as a source follower only when V_1 goes high. When V_1 goes low, Q_3 discharges V_b at a linear rate.

3.2. RL_2

Fig. 9 shows a second version of the retino-laminar circuit, RL_2. The difference between this circuit and RL_1 is that Q_3 in the biasing circuit is diode connected and the source of the transistor is brought out externally via V_s. This version was suggested by Rahul Sarpeshkar [4]. The transfer function of this circuit is similar to that of RL_1, except that the conductance, g_a, has a different dependence on the photocurrent, I_{ph}.

3.2.1 I–V Relationship. We do an analysis similar to that in Section 3.1.2, to determine the dependence of g_a on the photocurrent, I_{ph}. The equation governing the bias circuit is

$$\begin{aligned} I_b &= I_{on} e^{\kappa_n(\overline{V}+\Delta V/2)} e^{-V_b} \\ &= I_{on} e^{\kappa_n V_b - V_s} \end{aligned} \tag{14}$$

where $V_1 = \overline{V} + \Delta V/2$. We rearrange the terms in equation (14) to solve for $e^{-\kappa_p V_b}$:

$$e^{-\kappa_p V_b} = e^{(-\kappa_n\kappa_p/\kappa_n+1)(\overline{V}+\Delta V/2)} e^{-(\kappa_p/\kappa_n+1)V_s} \tag{15}$$

Substituting equation (15) into equation (8) (Section 3.1.2), and substituting for $\overline{V} = V_1 + V_{pl}/2 = V_{pl} + \Delta V/2$, we get

$$\begin{aligned} I &= 2I_{op} e^{(1-\kappa_n\kappa_p/(\kappa_n+1))\overline{V}} e^{-(\kappa_n\kappa_p/(\kappa_n+1))\Delta V/2} \sinh(\Delta V/2) e^{-(\kappa_p/\kappa_n+1)V_s} \\ &= 2I_{op} e^{(1-\kappa_n\kappa_p/(\kappa n+1))V_{pl}} e^{(1-2\kappa_n\kappa_p/(\kappa_n+1))\Delta V/2} \sinh(\Delta V/2) e^{-(\kappa_p/(\kappa_n+1))V_s} \end{aligned} \tag{16}$$

We now substitute in I_{ph} from equation (12):

$$I = I_\beta I_{ph}^{(1-\kappa_n\kappa p/(\kappa_n+1))/\kappa_n} e^{(1-2\kappa_n\kappa p/(\kappa_n+1))\Delta V/2} \sinh(\Delta V/2) e^{-(\kappa_p/(\kappa_n+1))V_s} \tag{17}$$

where $I_\beta = 2I_{op}\left(\frac{e^{V_T}}{I_{on}}\right)^{(1-\kappa_n\kappa_p/(\kappa_n+1))/\kappa_n}$.

The frequency-response curves for this circuit are shown in Fig. 10. These curves are similar to the

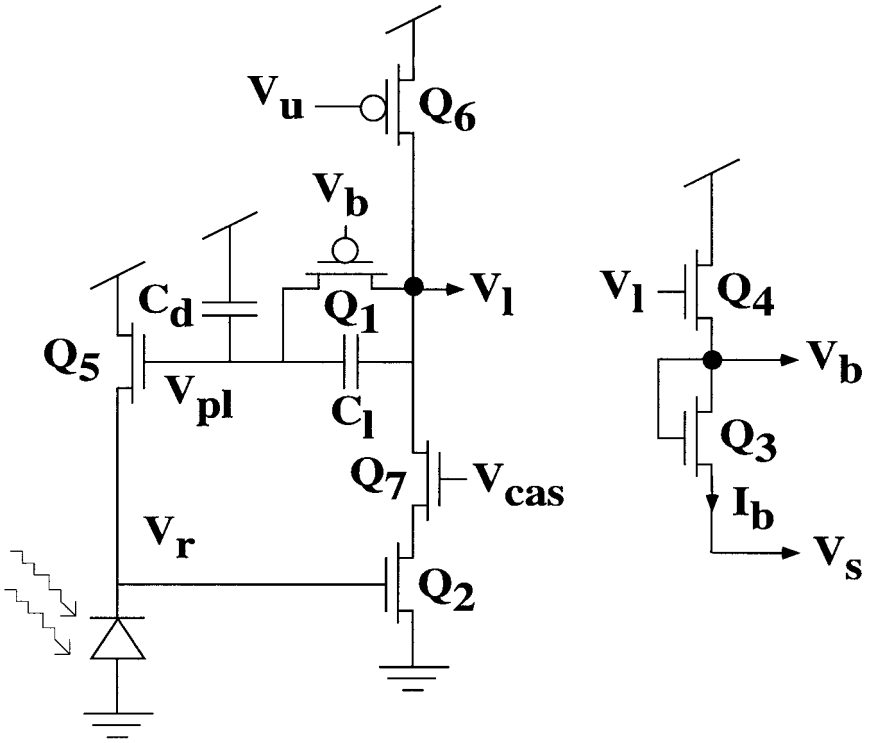

Fig. 9. Circuit diagram of the variant, RL_2. This circuit is the same as the RL_1 circuit, except that the biasing circuit is different. Here, the transistor, Q_3 is diode connected.

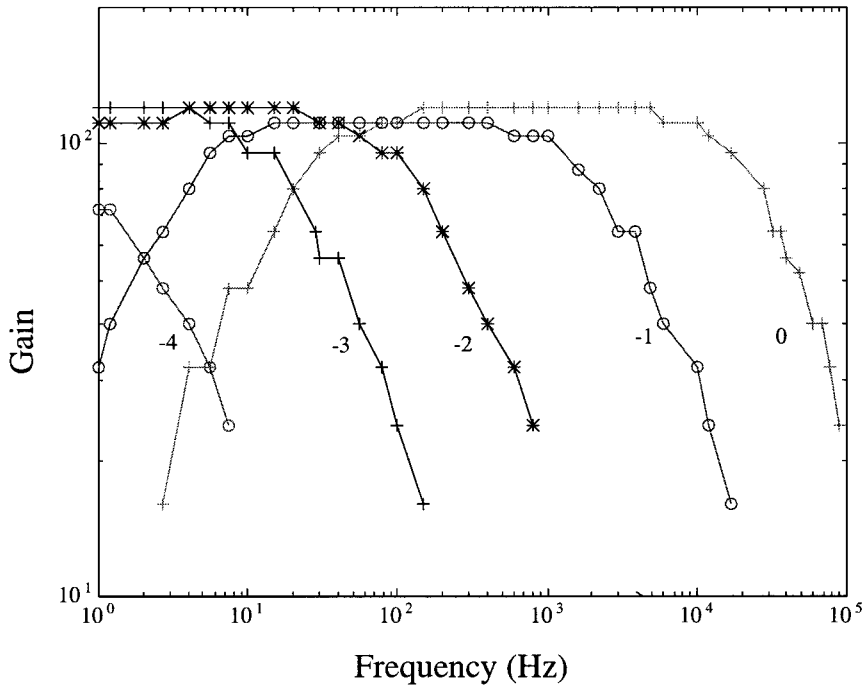

Fig. 10. Frequency plot of the RL_2 circuit over five decades of background intensity. The curves show that, in the range of 1 to 100 Hz, the circuit acts as a highpass filter for high light levels and as a lowpass filter under low light levels.

frequency-response curves of RL_1. As in Fig. 4, the circuit acts as a highpass filter under high light levels in the frequency range of 1 to 100 Hz, and reduces to a lowpass filter as the background intensity decreases.

3.2.2. Temporal Responses. A dependence of the temporal filtering of RL_2 on the background intensity similar to that of RL_1 can be seen in Fig. 11. Here, the figure shows the step responses of the RL_1 and RL_2 circuits to a square-wave-modulated LED of contrast 0.178 over four decades of background intensity. The top set of curves shows the responses from the RL_2 circuit; the bottom set of curves shows the responses from the RL_1 circuit. The biases, V_s and V_m, have been set such that the time constant for both circuits is approximately equal at the largest background intensity. Since Q_3 of the bias circuit of RL_2 is diode connected, the I_b current flowing through Q_3 is dependent on V_1 (or I_{ph}). Hence the temporal filtering of RL_2 has a bigger dependence on the background intensity than does the temporal filtering of RL_1.

3.2.3. Adaptation Properties. A comparison of the adaptation behaviors of both variants is shown in Fig. 12. The top curve shows the adaptive behavior of RL_2; the bottom curve shows the response from RL_1. The adaptation response is symmetrical for both RL_1 and RL_2, when the circuit goes from dark to light conditions and back. The dynamics of the adaptation is slightly different between both circuits at low intensities. The adaptation time constant of the RL_2 circuit can also be controlled externally via V_s. In Fig. 13, the adaptation behavior of RL_2 is shown for two different values of V_s. The bottom curve shows the response of the circuit with a higher value of V_s. A higher value of V_s corresponds to a decrease in the conductance, g_a, or an increase in the adaptation time constant.

4. 2-D Results

An imager consisting of a 20 × 20 array of RL_1 pixels was fabricated in 1.2 μm ORBIT CMOS nwell technology. An input stimulus consisting of a rotating flywheel, with black strips on a white background, was initially presented to the imager. The flywheel was then stopped, and the response of the chip was

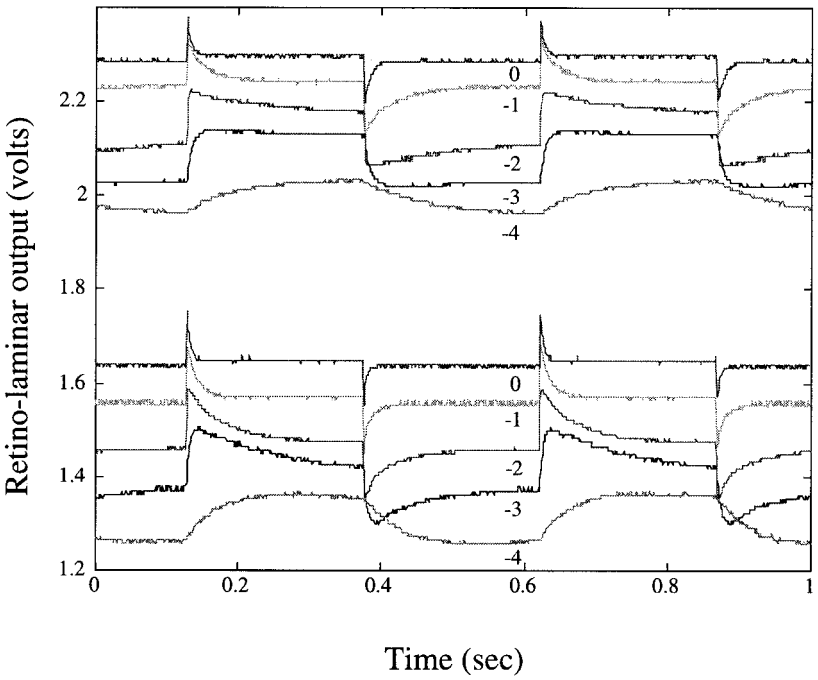

Fig. 11. Temporal responses of the RL_1 and RL_2 circuits. The curves show the responses of both variants over four decades of background intensity to a square-wave-modulated LED of contrast 0.178. The top set of curves shows the responses from RL_2, while the bottom set of curves shows the responses from RL_1. The biases, V_m and V_s, have been adjusted such that the time constants of both circuits at the highest intensity are about equal.

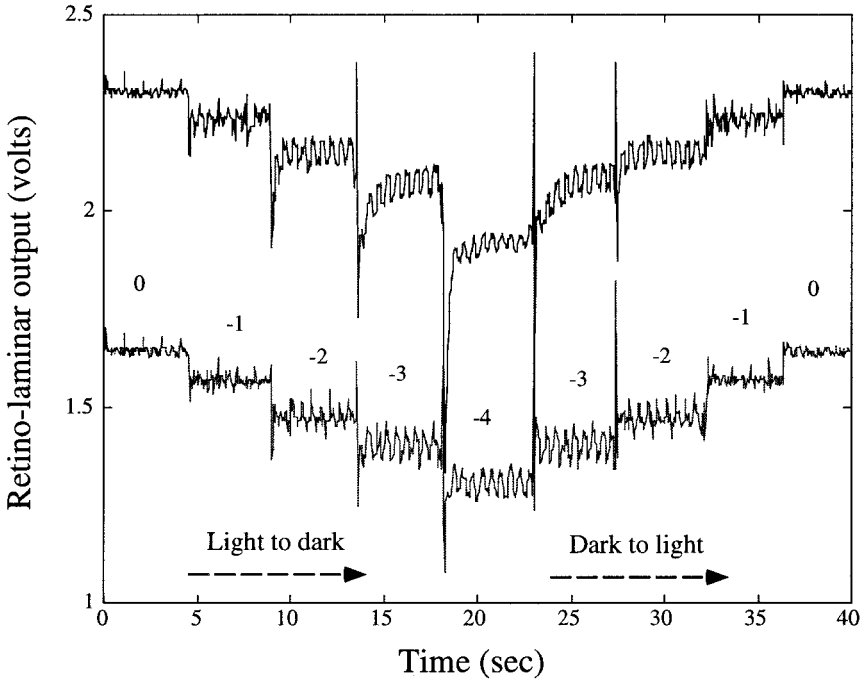

Fig. 12. Plots of adaptation responses of RL_1 and RL_2 under five decades of background intensity. The input stimulus is a square-wave-modulated LED of contrast 0.18. The top curve corresponds to the response from RL_2. The bottom curve corresponds to the response from RL_1.

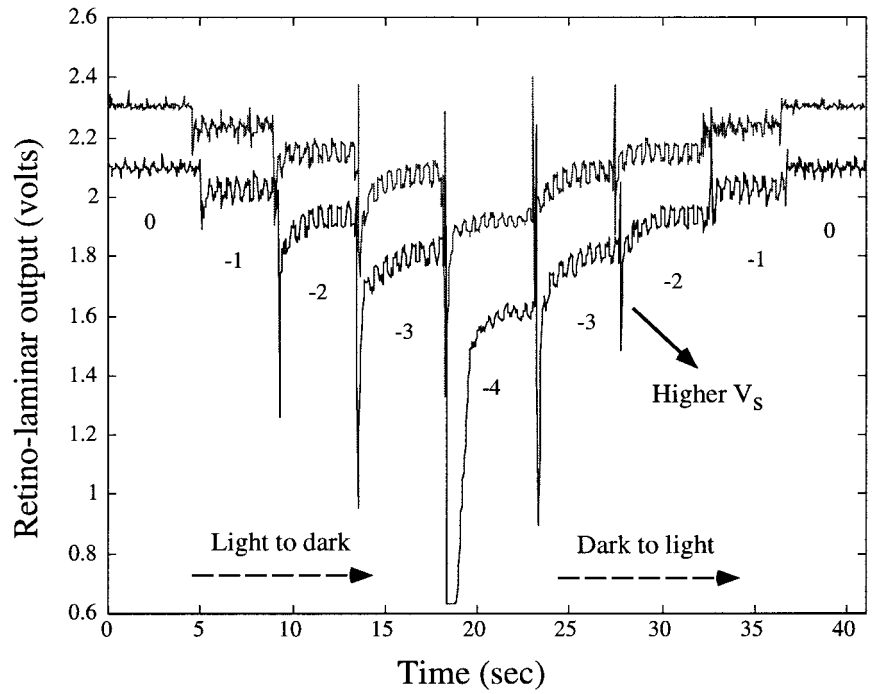

Fig. 13. Adaptation responses of RL_2 for two different values of V_s. The bottom curve corresponds to a higher value of V_s. The curve has been shifted down by 0.2 V for ease of comparison. A higher value of V_s corresponds to a decrease in conductance of Q_1, or to an increase in the adaptation time constant.

recorded one sec after the motion was ceased. I repeated the experiment for two adaptation time constants by changing the value of V_m. The image in Fig. 14(a) shows the output of the chip with the longer adaptation time constant. We see that the image is still present, whereas the image in Fig. 14(b) has almost faded away; that is, the chip has adapted away the stationary image.

5. Conclusions

I have described two versions of the RL circuit that capture the temporal and adaptation properties of both the photoreceptor and the laminar layers in the fly retina. By adapting to the background intensity, the RL circuit maintains a high transient gain. The temporal filtering of the circuit also changes with the background intensity, such that, at high S/N ratios, the circuit acts as a highpass filter and, at low S/N ratios, the circuit acts as a lowpass filter to average out the noise. The dependence of the temporal filtering on the background intensity is analogous to the dependence of the spatial filtering on the background intensity of the vertebrate retina. The circuit uses only six transistors and two capacitors. The adaptation time constant of the circuit can be controlled via an external bias.

6. Acknowledgment

I thank Bradley A. Minch for discussions of this work, Carver Mead for supporting this work, and the MOSIS foundation for fabricating this circuit. I also thank Lyn Dupre for editing this document. This work was supported in part by the Office of Naval Research, by DARPA, and by the Beckman Foundation. A large part of this work was completed in the Computation and Neural Systems Program at California Institute of Technology.

References

1. T. Delbrück, ''Analog VLSI phototransduction by continous-time, adaptive, logarithmic photoreceptor circuits.'' *CNS Memo No.30* California Institute of Technology, Pasadena, CA, 1994.
2. M. Juusola, R. O. Uusitola, and M. Weckstrom, ''Transfer of graded potentials at the photoreceptor-interneuron synapse.'' *J. of General Physiology* 105, pp. 115–148, 1995.
3. M. Banu and Y. Tsividis, ''Floating voltage-controlled resistors in CMOS technology.'' *Electronics Letters* 18(15), pp. 678–679, 1982.
4. R. Sarpeshkar, Personal communication, 1997.

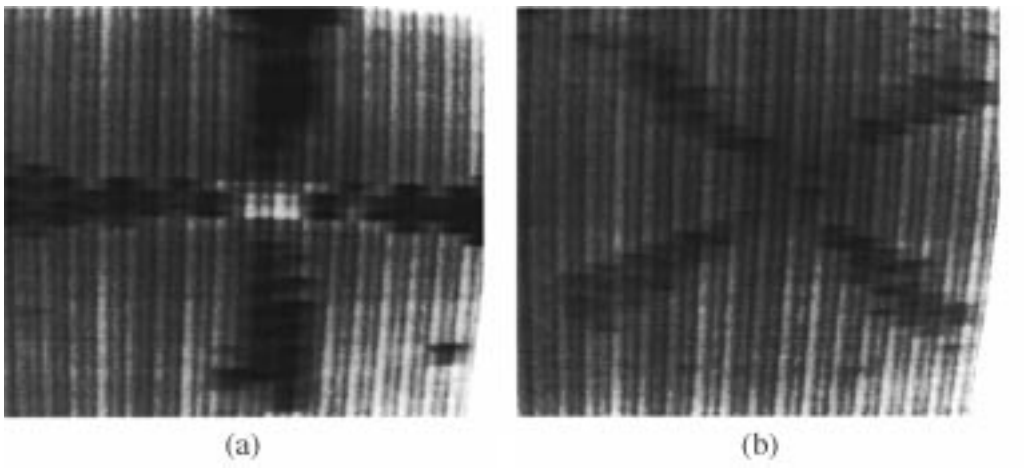

Fig. 14. Adaptation results from a two-dimensional array of 20 × 20 pixels. The output of the array was recorded one sec after cessation of the pattern motion. The experiment was repeated for two different adaptation time constants. Fig. (a) corresponds to the longer adaptation time constant. The image is still present, whereas the image in Fig. (b) has almost faded away.

Shih-Chii Liu received the B.Sc. degree in Electrical Engineering from Massachusetts Institute of Technology, Cambridge, in 1983, and the M.S. degree in Electrical Engineering from UCLA in 1988. She received the Ph.D. degree in the Computation and Neural Systems Program from California Institute of Technology in 1997. She is currently on the research staff in the Computation and Neural Systems Program at California Institute of Technology.

Dr. Liu was with Gould American Microsystems from 1983 to 1985, and with LSI Logic from 1985 to 1988. She was with Rockwell International Research Labs from 1988 to 1997. Her research interests include neuromorphic modeling of biological visual systems using analog VLSI circuits. She is a member of Eta Kappa Nu.